Article

aeroacoustics

International Journal of Aeroacoustics
2020, Vol. 19(1–2) 38–56

DOI: 10.1177/1475472X20905043
journals.sagepub.com/home/jae
SAGE

Diffraction of sound waves by a lined cylindrical cavity

Burhan Tiryakioglu

Abstract

In this paper, diffraction of sound waves through a lined cavity is analyzed rigorously. The inner–outer surfaces of the cavity and the base of the cavity are coated with three different absorbing linings. By using the Fourier transform technique in conjunction with the Mode-Matching method, the related boundary value problem is formulated as a Wiener–Hopf equation. In the solution, two infinite sets of unknown coefficients are involved that satisfy two infinite systems of linear algebraic equations. Numerical solution of this system is obtained for various values of the parameters of the problem. The graphical results are also presented which show that how efficiently the sound diffraction can be reduced by selection of problem parameters.

Keywords

Wiener–Hopf, Fourier transform, cavity, Mode Matching, absorbing lining

Date received: 2 April 2019; revised 28 August 2019; accepted: 10 December 2019

Introduction

Waveguide cavities are a well-known subject in acoustic, physics, and electromagnetic. It has attracted the attention of various investigators working in the field.[1–4] In particular, diffraction of sound by open-ended waveguide cavities is a significant topic in noise reduction and in radar target scattering. A lot of options for the reduction of noise have been discussed extensively in the literature. The notion of absorbing lining is considered to be the most convenient way of reducing unwanted sound. Rawlins proved that acoustically absorbing lining is an efficient method to reduce the irritated sound. He analyzed the radiation of sound from an unflanged rigid cylindrical duct with an acoustically absorbing internal surface.[5] The phenomenon of diffraction with acoustically absorbing lining has also been investigated with and without flow by various researchers.[6–11]

Department of Applied Mathematics, Marmara University, Istanbul, Turkey

Corresponding author:
Burhan Tiryakioglu, Department of Applied Mathematics, Marmara University, Istanbul 34722, Turkey.
Email: burhan.tiryakioglu@marmara.edu.tr

Demir et al. studied the diffraction plane sound waves by a rigid circular cylindrical cavity with an acoustically internal surface.[12] In their study, a hybrid method was applied successfully to the solution and some numerical results were also given graphically. A similar problem has been considered for some engineering applications. Matsui discussed the diffraction phenomena of plane sound waves by the actual microphone system.[13] In the literature, parallel problem which is related to the electromagnetic counterpart was studied by Kuryliak et al.[14,15]

This work was conceived by generalizing the study of Demir et al.[12] Here, three different admittances for outer–inner surfaces and base of the cavity were used. We intend to discover diffraction properties of the absorbing lining and the effect of outer surface admittance. By expressing the total field in the cavity region in terms of normal waveguide modes and using the Fourier transform elsewhere, the related boundary value problem is solved analytically with the help of sophisticated and suitable method known as Wiener–Hopf technique.[16] Since the formulation based on the Mode-Matching method in conjunction with the Fourier transform technique is adopted, this mixed formulation yields a scalar Wiener–Hopf equation. The solution of the Wiener–Hopf equation involves infinitely many unknown coefficients satisfying two infinite systems of linear algebraic equations. Numerical solution of these systems is obtained for various values of the parameters of the problem such as cavity radius, cavity depth, and surface admittances, and their effects on the diffraction phenomenon are shown graphically.

This study is sorted in the following order. In section "Analysis", the mathematical model is formulated. The Wiener–Hopf equation, which is obtained using a standard Wiener–Hopf procedure, is developed with the help of Fourier transform technique in conjunction with the Mode-Matching method. The solution of the Wiener–Hopf problem, expansion coefficients, and far field are also presented in section "Analysis". The graphs with various parameters are displayed and discussed in section "Computational results". To end with, concluding remarks are summarized in section "Concluding remarks".

The time dependence is assumed to be $e^{-i\omega t}$ and suppressed through the paper, where ω is the angular frequency.

Analysis

Consider the diffraction of sound waves by a semi-infinite lined circular cylindrical cavity defined by $\{\rho = a, z \in (-\infty, 0)\}$ (see Figure 1) where (ρ, ϕ, z) denote the usual cylindrical polar coordinates. The outer surface of the semi-infinite cylinder $\{\rho = a + 0, z \in (-\infty, 0)\}$ is assumed to be lined with an acoustically absorbent material having a surface admittance β_1 while the inner surface of the cavity $\{\rho = a - 0, z \in (-l, 0)\}$ and the base of the cavity $\{z = -l + 0, \rho \in (0, a)\}$ are coated by another acoustically absorbent material which is characterized by a surface admittances β_2 and β_3, respectively.

From the symmetry of the geometry of the problem and of the incident field, the acoustic field everywhere will be independent of ϕ. We shall therefore introduce a scalar potential $u(\rho, z)$ which defines the acoustic pressure and velocity by $p = i\omega\rho_0 u$ and $v = \text{grad}u$, respectively, where ρ_0 is the density of the undisturbed medium. Due to the boundary conditions of the geometry of the problem, the incident field is taken to be

$$u_i(\rho, z) = A_0 J_0(\gamma_m \rho / a) e^{-i\alpha_m z} \tag{1a}$$

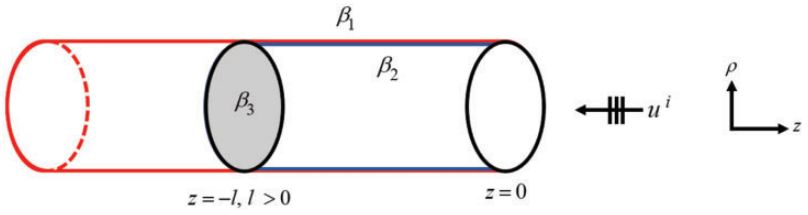

Figure 1. Geometry of the problem.

where γ_m is the root of the equation

$$ika\beta_1 J_0(\gamma_m) - \gamma_m J_1(\gamma_m) = 0 \tag{1b}$$

and α_m stands for

$$\alpha_m = \sqrt{k^2 - (\gamma_m/a)^2} \tag{1c}$$

where $k = \omega/c$ denotes the wave number and c is the speed of the sound. A_0 stands for the amplitude of the incident wave which will be taken equal to 1 in the analysis. For the sake of analytical convenience, we will assume that the surrounding medium is slightly lossy and k has a small positive imaginary part. The lossless case can be obtained by letting $Imk \to 0$ at the end of the analysis. The total field $u^T(\rho, z)$ can be written as

$$u^T(\rho,z) = \begin{cases} u_1(\rho,z) + u_i; & \rho > a, z \in (-\infty, \infty) \\ u_2(\rho,z) + u_i; & \rho < a, 0 < z < \infty \\ u_3(\rho,z); & \rho < a, -l < z < 0 \end{cases} \tag{2}$$

$u_j, j = 1, 2, 3$, which satisfy the Helmholtz equation, are to be determined with the aid of the following boundary and continuity relations. The boundary condition on the absorbent surface can be given in terms of the potential functions

$$\left(ik\beta_1 + \frac{\partial}{\partial\rho}\right) u_1(a,z) = 0, \quad z < 0 \tag{3a}$$

$$\left(ik\beta_2 - \frac{\partial}{\partial\rho}\right) u_3(a,z) = 0, \quad -l < z < 0 \tag{3b}$$

$$\left(ik\beta_3 + \frac{\partial}{\partial z}\right) u_3(\rho,-l) = 0, \quad 0 < \rho < a \tag{3c}$$

Consider now the continuity conditions related to total field at $\rho < a$, $z > 0$ which are given by

$$\frac{\partial}{\partial\rho} u_1(a,z) - \frac{\partial}{\partial\rho} u_2(a,z) = 0, \quad z > 0 \tag{3d}$$

$$u_1(a,z) - u_2(a,z) = 0, \quad z > 0 \tag{3e}$$

From the continuity at the point $z = 0$, we get

$$\frac{\partial}{\partial z} u_2(\rho,0) + \frac{\partial}{\partial z} u_i(\rho,0) = \frac{\partial}{\partial z} u_3(\rho,0), \quad \rho < a \tag{3f}$$

$$u_2(\rho,0) + u_i(\rho,0) = u_3(\rho,0), \quad \rho < a \tag{3g}$$

Furthermore, to obtain a unique solution, the following edge conditions at the mouth $\rho = a$, $z = 0$ of the cylinder should be taken into account

$$u_1 = Cons \tag{4a}$$

$$\frac{\partial}{\partial \rho} u_1 = o(z^{-1/2}) \tag{4b}$$

Wiener–Hopf equation

The fields u_j, $j = 1, 2, 3$ satisfy the Helmholtz equation for $z \in (-\infty, \infty)$

$$\left[\frac{1}{\rho}\frac{\partial}{\partial \rho}\left(\rho \frac{\partial}{\partial \rho}\right) + \frac{\partial^2}{\partial z^2} + k^2\right] u_j(\rho,z) = 0, \quad j = 1,2,3 \tag{5}$$

Consider the Fourier transform of the Helmholtz equation satisfied by $u_1(\rho,z)$ in the region $\rho > a$ for $z \in (-\infty, \infty)$

$$\left[\frac{1}{\rho}\frac{\partial}{\partial \rho}\left(\rho \frac{\partial}{\partial \rho}\right) + K^2(\alpha)\right] F(\rho,\alpha) = 0 \tag{6a}$$

where $K(\alpha)$ is the square root function

$$K(\alpha) = \sqrt{k^2 - \alpha^2}, \quad K(0) = k \tag{6b}$$

which is defined in the complex $\alpha-$ plane (see Figure 2) and $F(\rho,\alpha)$ is the Fourier transform of the field $u_1(\rho,z)$ defined to be

$$F(\rho,\alpha) = \int_{-\infty}^{\infty} u_1(\rho,z) e^{i\alpha z} \mathrm{d}z = F^{-}(\rho,\alpha) + F^{+}(\rho,\alpha) \tag{7}$$

with

$$F^{-}(\rho,\alpha) = \int_{-\infty}^{0} u_1(\rho,z) e^{i\alpha z} \mathrm{d}z \tag{8a}$$

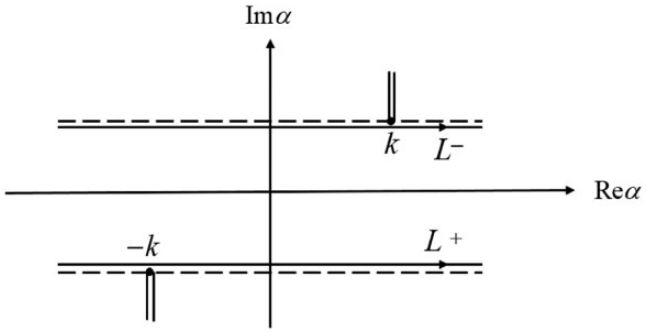

Figure 2. Complex α– plane.

$$F^{+}(\rho,\alpha)=\int_{0}^{\infty}u_1(\rho,z)e^{i\alpha z}\mathrm{d}z \tag{8b}$$

Through the analytical properties of Fourier integrals, $F^{+}(\rho,\alpha)$ and $F^{-}(\rho,\alpha)$ are regular functions in the upper half plane $(\Im m\alpha > \Im m(-k))$ and in the lower half plane $(\Im m\alpha < \Im mk)$, respectively. The general solution of equation (6a) yields

$$F^{-}(\rho,\alpha)+F^{+}(\rho,\alpha)=A(\alpha)H_0^{(1)}(K\rho) \tag{9}$$

where $A(\alpha)$ is a spectral coefficient to be determined and $H_0^{(1)}$ is the Hankel function of the first type. Consider now the Fourier transform of equation (3a), we get

$$ik\beta_1F^{-}(a,\alpha)+\dot{F}^{-}(a,\alpha)=0 \tag{10}$$

where the dot specifies the derivative with respect to ρ. Multiplying equation (9) with $ik\beta_1$ and taking the derivative of equation (9) with respect to ρ, one can write the following equation at $\rho=a$,

$$ik\beta_1F^{-}(a,\alpha)+\dot{F}^{-}(a,\alpha)+ik\beta_1F^{+}(a,\alpha)+\dot{F}^{+}(a,\alpha)=A(\alpha)\left[ik\beta_1H_0^{(1)}(Ka)-KH_1^{(1)}(Ka)\right] \tag{11a}$$

Utilizing equation (10) in equation (11a), we obtain

$$W^{+}(\alpha)=A(\alpha)H(\alpha) \tag{11b}$$

where

$$W^{+}(\alpha)=ik\beta_1F^{+}(a,\alpha)+\dot{F}^{+}(a,\alpha) \tag{12}$$

$$H(\alpha)=ik\beta_1H_0^{(1)}(Ka)-KH_1^{(1)}(Ka) \tag{13}$$

Inserting equation (11b) into equation (9) we get

$$F^{-}(\rho,\alpha)+F^{+}(\rho,\alpha)=W^{+}(\alpha)\frac{H_0^{(1)}(K\rho)}{H(\alpha)} \tag{14}$$

Now consider the region $\rho<a,\ z>0$. The field $u_2(\rho,z)$ satisfies the Helmholtz equation for $z\in(0,\infty)$ as denoted (equation (5)). The Fourier transform of this equation for $\rho<a,\ z>0$ is

$$\left[\frac{1}{\rho}\frac{\partial}{\partial\rho}\left(\rho\frac{\partial}{\partial\rho}\right)+K^2(\alpha)\right]G^{+}(\rho,\alpha)=f(\rho)-i\alpha g(\rho) \tag{15}$$

where $G^{+}(\rho,\alpha)$ is a regular function in the upper half plane, defined by

$$G^{+}(\rho,\alpha)=\int_0^{\infty}u_2(\rho,z)e^{i\alpha z}\mathrm{d}z \tag{16}$$

with

$$f(\rho)=\frac{\partial}{\partial z}u_2(\rho,0),\quad g(\rho)=u_2(\rho,0) \tag{17a,b}$$

The particular solution of equation (15), which is bounded at $\rho=0$ and satisfying equation (3a) can be obtained by the Green's function technique. The Green function of equation (15) satisfies the Helmholtz equation.

$$\left[\frac{1}{\rho}\frac{\partial}{\partial\rho}\left(\rho\frac{\partial}{\partial\rho}\right)+K^2(\alpha)\right]\tilde{G}(\rho,t,\alpha)=0\quad\rho\neq t,\quad\rho,t\in(0,a) \tag{18}$$

with the following conditions

$$\tilde{G}(0,t,\alpha)\sim\text{bounded} \tag{19a}$$

$$\tilde{G}(t+0,t,\alpha)-\tilde{G}(t-0,t,\alpha)=0 \tag{19b}$$

$$\frac{\partial}{\partial\rho}\tilde{G}(t+0,t,\alpha)-\frac{\partial}{\partial\rho}\tilde{G}(t-0,t,\alpha)=\frac{1}{t} \tag{19c}$$

$$\left(ik\beta_1+\frac{\partial}{\partial\rho}\right)\tilde{G}(a,t,\alpha)=0 \tag{19d}$$

The solution of equation (18) under the conditions given above is

$$\tilde{G}(\rho,t,\alpha)=\frac{1}{J(\alpha)}Q(\rho,t,\alpha) \tag{20a}$$

with

$$Q(\rho,t,\alpha)=\frac{\pi}{2}\begin{cases}J_0(K\rho)\big[J(\alpha)Y_0(Kt)-Y(\alpha)J_0(Kt)\big], & \rho<t\\ J_0(Kt)\big[J(\alpha)Y_0(K\rho)-Y(\alpha)J_0(K\rho)\big], & \rho>a\end{cases} \tag{20b}$$

where J_0 and Y_0 are the Bessel and Neumann functions of order zero and $J(\alpha)$, $Y(\alpha)$ are given below

$$J(\alpha)=ik\beta_1 J_0(Ka)-KJ_1(Ka) \tag{21a}$$

$$Y(\alpha)=ik\beta_1 Y_0(Ka)-KY_1(Ka) \tag{21b}$$

Hence, the general solution of equation (15) can be expressed as

$$G^+(\rho,\alpha)=\frac{B(\alpha)J_0(K\rho)}{J(\alpha)}+\frac{1}{J(\alpha)}\int_0^a (f(t)-i\alpha g(t))Q(t,\rho,\alpha)t\mathrm{d}t \tag{22}$$

where $B(\alpha)$ is the spectral coefficient to be determined. Taking into account the continuity relation equation (3d) and equation (3e), one gets

$$B(\alpha)=ik\beta_1 G^+(a,\alpha)+\dot{G}^+(a,\alpha)=ik\beta_1 F^+(a,\alpha)+\dot{F}^+(a,\alpha)=W^+(\alpha) \tag{23}$$

which yields

$$G^+(\rho,\alpha)=\frac{W^+(\alpha)J_0(K\rho)}{J(\alpha)}+\frac{1}{J(\alpha)}\int_0^a (f(t)-i\alpha g(t))Q(t,\rho,\alpha)t\mathrm{d}t \tag{24}$$

Although the left-hand side of equation (24) is analytic in the upper half plane, the regularity of the right-hand side is violated by the presence of simple poles occurring at the zeros of $J(\alpha)$ lying in the upper half plane, which are defined in equations (1b) and (1c). In order to provide regularity of the right-hand side of equation (24) in the upper half plane, these poles must be eliminated by imposing that their residues are zero. This gives

$$W^+(\alpha_m)=\frac{a}{2}J_0(\gamma_m)\Big[1-(\beta_1 ka/\gamma_m)^2\Big][f_m-i\alpha_m g_m] \tag{25}$$

with

$$\begin{bmatrix}f_m\\ g_m\end{bmatrix}=\frac{2}{a^2J_0^2(\gamma_m)\Big[1-(\beta_1 ka/\gamma_m)^2\Big]}\int_0^a\begin{bmatrix}f(t)\\ g(t)\end{bmatrix}J_0\left(\frac{\gamma_m}{a}t\right)t\mathrm{d}t \tag{26}$$

Let us expand and into Dini series[17] as follows

$$f(\rho)=\sum_{m=1}^{\infty}f_m J_0\left(\frac{\gamma_m}{a}\rho\right),\quad g(\rho)=\sum_{m=1}^{\infty}g_m J_0\left(\frac{\gamma_m}{a}\rho\right) \tag{27a,b}$$

Now consider the Fourier transform of the continuity relation (equation (3e)), one gets

$$G^{+}(a,\alpha) = F^{+}(a,\alpha) \tag{28}$$

Taking into account equations (24) and (14), we obtain

$$\frac{W^{+}(\alpha)}{M(\alpha)} - \frac{a}{2}F^{-}(a,\alpha) = -\frac{1}{2J(\alpha)}\int_0^a (f(t) - i\alpha g(t))J_0(Kt)t\mathrm{d}t \tag{29}$$

where

$$M(\alpha) = \pi i J(\alpha)H(\alpha) \tag{30}$$

The evaluation of the integral at the right-hand side of equation (29) after inserting equation (27a,b) in equation (29), we obtain the following Wiener–Hopf equation valid in the strip $\Im m(-k) < \Im m\alpha < \Im mk$.

$$\frac{W^{+}(\alpha)}{M(\alpha)} - \frac{a}{2}F^{-}(a,\alpha) = \frac{a}{2}\sum_{m=1}^{\infty}\frac{J_0(\gamma_m)}{\alpha_m^2 - \alpha^2}[f_m - i\alpha g_m] \tag{31}$$

Solution of the Wiener–Hopf equation

By using the Wiener–Hopf factorization method, the kernel function can be written as[16]

$$M(\alpha) = M_{+}(\alpha)M_{-}(\alpha), \quad M_{-}(\alpha) = M_{+}(-\alpha) \tag{32a,b}$$

where $M_{+}(\alpha)$ and $M_{-}(\alpha)$ are the split functions regular and free of zeros in the upper and lower halves of the complex plane, respectively. Note that, when we let $|\alpha| \to \infty$ in their respective regions of regularity, we have

$$M_{\pm}(\alpha) = \mathcal{O}(\pm\alpha^{1/2}) \tag{32c}$$

The explicit expression for $M_{+}(\alpha)$ is given in Tiryakioglu and Demir[18] as

$$\begin{aligned} M_{+}(\alpha) = {} & \sqrt{\pi i\left(ik\beta_1 J_0(ka) - kJ_1(ka)\right)}\sqrt{\left(ik\beta_1 H_0^{(1)}(ka) - kH_1^{(1)}(ka)\right)} \\ & \times \exp\left\{i\frac{a\alpha}{\pi}\left[1 - \zeta + \log\left(\frac{2\pi}{ka}\right) + i\frac{\pi}{2}\right] - \frac{ika}{2}\right\}\exp\left(\frac{aK(\alpha)}{\pi}\log\left(\frac{\alpha + iK(\alpha)}{k}\right) + q(\alpha)\right) \\ & \times \prod_{m=1}^{\infty}\left(1 + \frac{\alpha}{\alpha_m}\right)\exp\left(\frac{i\alpha a}{m\pi}\right) \end{aligned} \tag{33}$$

where ζ is the Euler's constant given by $\zeta = 0.57721\ldots$ and $q(\alpha)$ stands for

$$q(\alpha) = \frac{1}{\pi}P\int_0^{\infty}\left[1 - \frac{2}{\pi x}\frac{x^2 - (\beta_1 ka)^2}{\mu(x)}\right]\log\left(1 + \frac{\alpha a}{\sqrt{(ka)^2 - x^2}}\right)\mathrm{d}x \tag{34a}$$

$$\mu(x) = (i\beta_1 kaJ_0(x) - xJ_1(x))^2 + (i\beta_1 kaY_0(x) - xY_1(x))^2 \tag{34b}$$

The multiplication of both sides of equation (31) by $M_-(\alpha)$, we get

$$\frac{W^+(\alpha)}{M_+(\alpha)} - \frac{a}{2}F^-(a,\alpha)M_-(\alpha) = \frac{a}{2}M_-(\alpha)\sum_{m=1}^{\infty}\frac{J_0(\gamma_m)}{\alpha_m^2 - \alpha^2}[f_m - i\alpha g_m] \tag{35}$$

Decomposition of the right-hand side of equation (35) and applying the Liouville's theorem, the solution of equation (35) can easily be obtained in the following form

$$\frac{W^+(\alpha)}{M_+(\alpha)} = \frac{a}{2}\sum_{m=1}^{\infty}\frac{J_0(\gamma_m)[f_m + i\alpha_m g_m]M_+(\alpha_m)}{2\alpha_m(\alpha + \alpha_m)} \tag{36}$$

Determination of the expansion coefficients

The field in the cavity can be expressed in terms of the waveguide normal modes as follows

$$u_3(\rho, z) = \sum_{n=1}^{\infty}\left[a_n e^{-i\chi_n z} + b_n e^{i\chi_n z}\right]J_0\left(\frac{\xi_n}{a}\rho\right) \tag{37a}$$

Here ξ_n's are the roots of the characteristic equation

$$ika\beta_2 J_0(\xi_n) + \xi_n J_1(\xi_n) = 0, \quad n = 1, 2, \ldots \tag{37b}$$

while χ_n's stand for

$$\chi_n = \sqrt{k^2 - \left(\frac{\xi_n}{a}\right)^2}, \quad n = 1, 2, \ldots \tag{37c}$$

By using the boundary condition in equation (3c), equation (37a) reduces to

$$u_3(\rho, z) = \sum_{n=1}^{\infty}a_n\left[e^{-i\chi_n z} + R_n e^{i\chi_n z}\right]J_0\left(\frac{\xi_n}{a}\rho\right) \tag{38a}$$

with

$$R_n = -\frac{\beta_3 - \chi_n/k}{\beta_3 + \chi_n/k}e^{2i\chi_n l} \tag{38b}$$

Now, from the continuity relations equation (3f) and equation (3g), we write

$$f(\rho) = \frac{\partial}{\partial z}u_2(\rho, 0) = \frac{\partial}{\partial z}u_3(\rho, 0) + i\alpha_r A_0 J_0(\gamma_r\rho/a) \tag{39a}$$

$$g(\rho) = u_2(\rho, 0) = u_3(\rho, 0) - A_0 J_0(\gamma_r\rho/a) \tag{39b}$$

Inserting the series expansions of f(ρ) and g(ρ) given in equation (27a,b) in equations (39a) and (39b), respectively, and using equation (38a), we get

$$\sum_{m=1}^{\infty} f_m J_0\left(\frac{\gamma_m}{a}\rho\right) = i\sum_{n=1}^{\infty} a_n \chi_n [R_n - 1] J_0\left(\frac{\xi_n}{a}\rho\right) + i\alpha_r A_0 J_0(\gamma_r \rho/a) \tag{40a}$$

$$\sum_{m=1}^{\infty} g_m J_0\left(\frac{\gamma_m}{a}\rho\right) = \sum_{n=1}^{\infty} a_n [R_n + 1] J_0\left(\frac{\xi_n}{a}\rho\right) - A_0 J_0(\gamma_r \rho/a) \tag{40b}$$

Multiplying both sides of equations (40a) and (40b) by $\rho J_0(\xi_l \rho/a)$ and integrating from $\rho = 0$ to $\rho = a$, we obtain for $n = l$ the following system of linear algebraic equations

$$\sum_{m=1}^{\infty}\left[f_m - \frac{R_n - 1}{R_n + 1} i\chi_n g_m\right] \frac{J_0(\gamma_m)}{\xi_n^2 - \gamma_m^2}\left(1 + \frac{\beta_1}{\beta_2}\right) = \frac{iA_0 J_0(\gamma_r)}{\xi_n^2 - \gamma_r^2}\left[\alpha_r + \frac{R_n - 1}{R_n + 1}\chi_n\right] \tag{41a}$$

By substituting $\alpha = \alpha_1, \alpha_2, \alpha_3, \ldots$ in equation (36) and using equation (25), one can obtain

$$\frac{J_0(\gamma_r)\left[1 - (\beta_1 ka/\gamma_r)^2\right][f_r - i\alpha_r g_r]}{M_+(\alpha_r)} = \sum_{m=1}^{\infty} \frac{J_0(\gamma_m)[f_m + i\alpha_m g_m] M_+(\alpha_m)}{2\alpha_m(\alpha_r + \alpha_m)} \tag{41b}$$

Equations (41a) and (41b) are the required linear systems of algebraic equations which permit us to determine f_m and g_m.

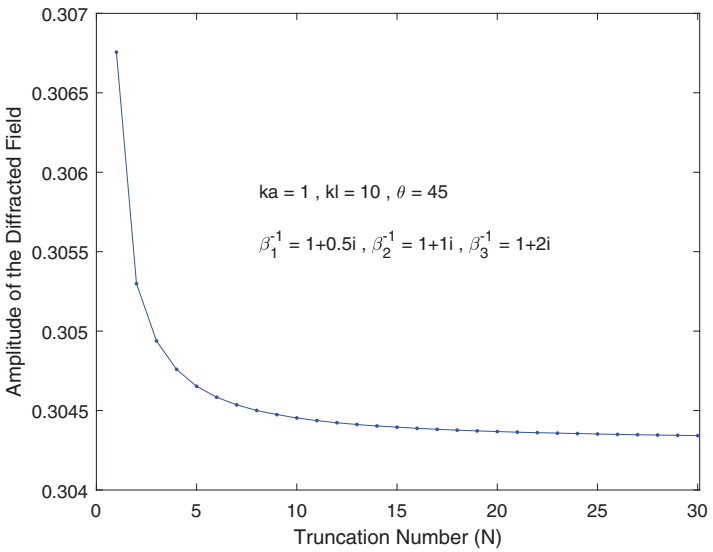

Figure 3. Diffracted field amplitude versus the truncation number *N*.

Far field

The diffracted field in the region $\rho > a$ can be obtained by taking the inverse Fourier transform of $F(\rho, \alpha)$. By using equation (14), we write

$$u_1(\rho, z) = \frac{1}{2\pi} \int_{\mathcal{L}} W^+(\alpha) \frac{H_0^{(1)}(K\rho)}{H(\alpha)} e^{-i\alpha z} \mathrm{d}\alpha \tag{42}$$

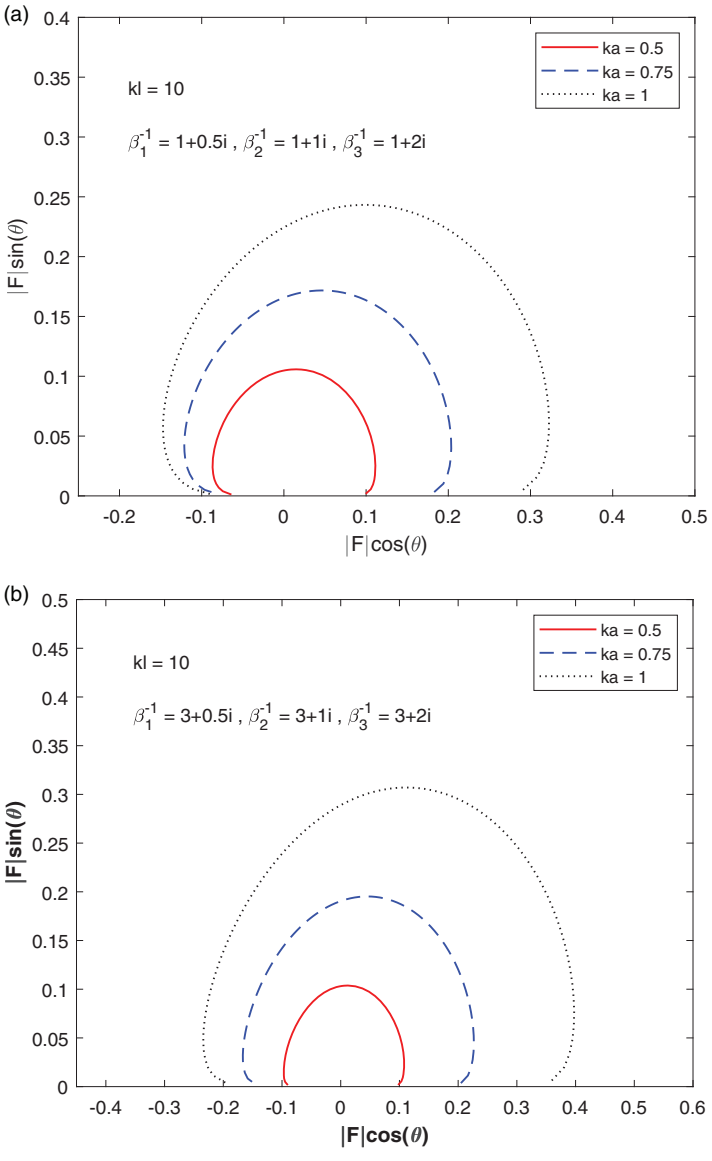

Figure 4. Amplitude of the diffracted field for different values of the cavity radius.

where $\mathcal{L}$ is a straight line parallel to the real α-axis, lying in the strip $\Im m(-k) < \Im m\alpha < \Im mk$. Utilizing the asymptotic expansion of $H_0^{(1)}(K\rho)$ as $k\rho \to \infty$

$$H_0^{(1)}(K\rho) = \sqrt{\frac{2}{\pi K\rho}} e^{iK\rho - i\pi/4} \tag{43}$$

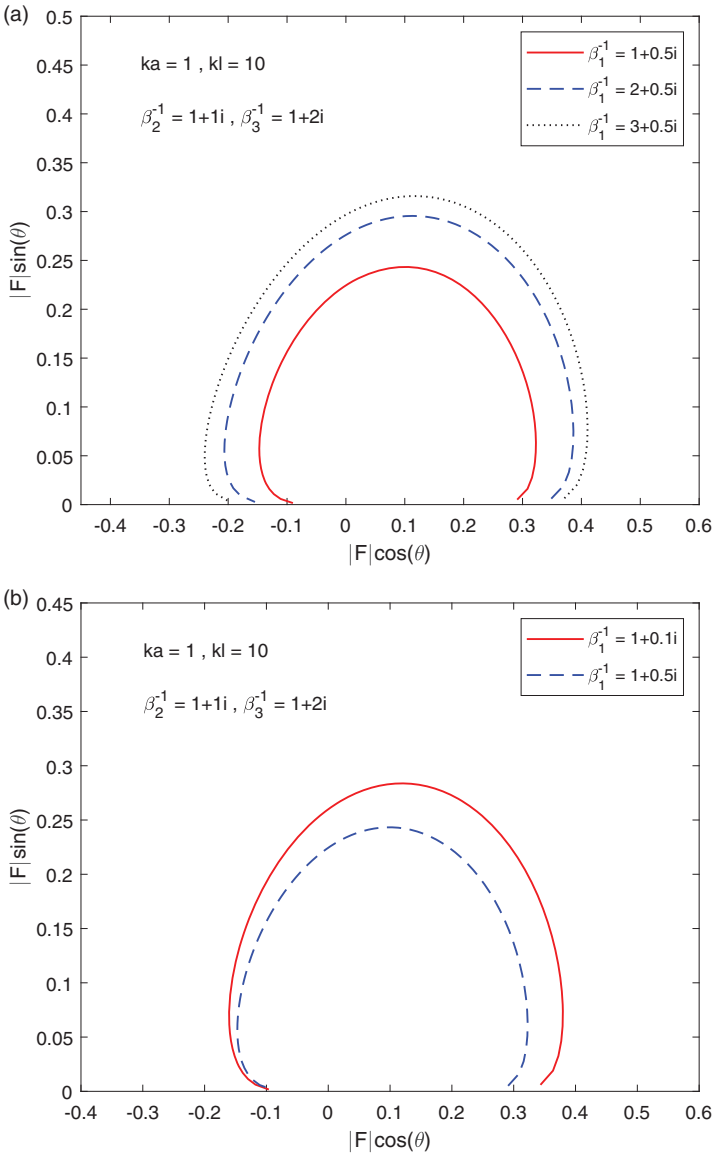

Figure 5. Amplitude of the diffracted field for different values of resistance $(\mathrm{Re}\beta_1^{-1})$ and reactance $(\mathrm{Im}\beta_1^{-1})$, respectively.

the asymptotic evaluation of the integral in equation (42) using the saddle point technique,[19] yields for the diffracted field

$$u_1(\rho, z) \sim \mathcal{F}(\theta)\frac{e^{ikr}}{kr} \tag{44a}$$

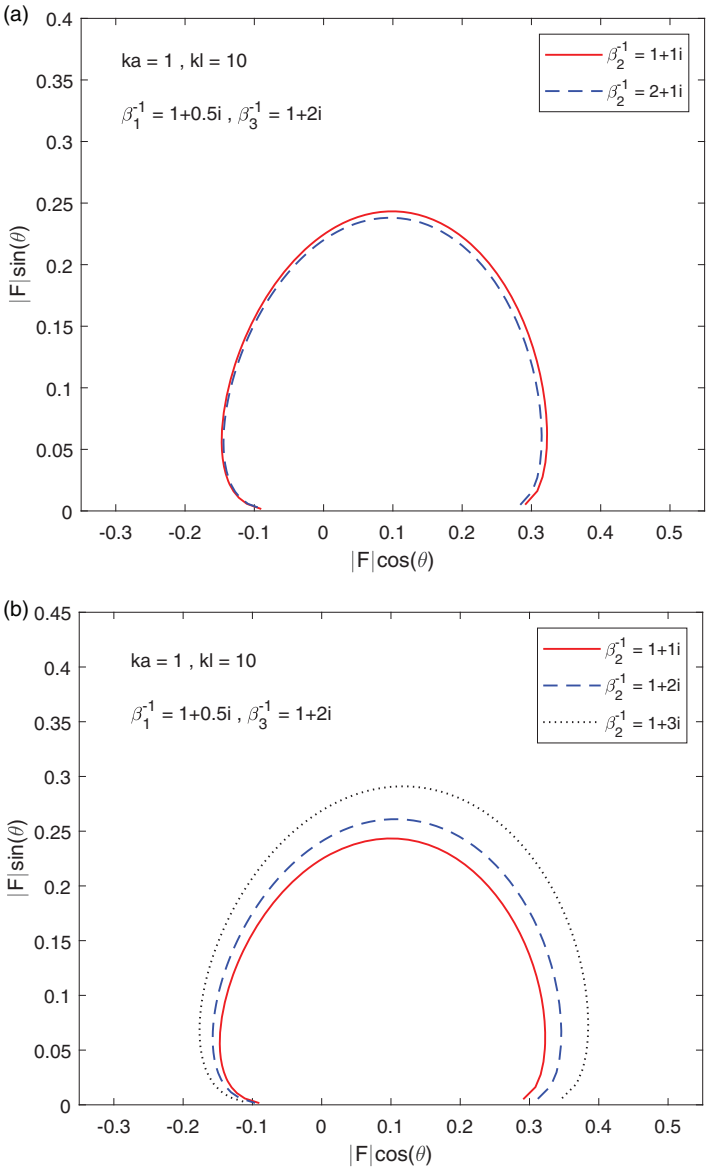

Figure 6. Amplitude of the diffracted field for different values of resistance $(\mathrm{Re}\beta_2^{-1})$ and reactance $(\mathrm{Im}\beta_2^{-1})$, respectively.

where

$$\mathcal{F}(\theta) = \frac{k}{i\pi} \frac{W^{+}(-k\cos\theta)}{H(-k\cos\theta)} \tag{44b}$$

Here r and θ are the spherical coordinates defined by

$$\rho = r\sin\theta, \quad z = r\cos\theta \tag{45a,b}$$

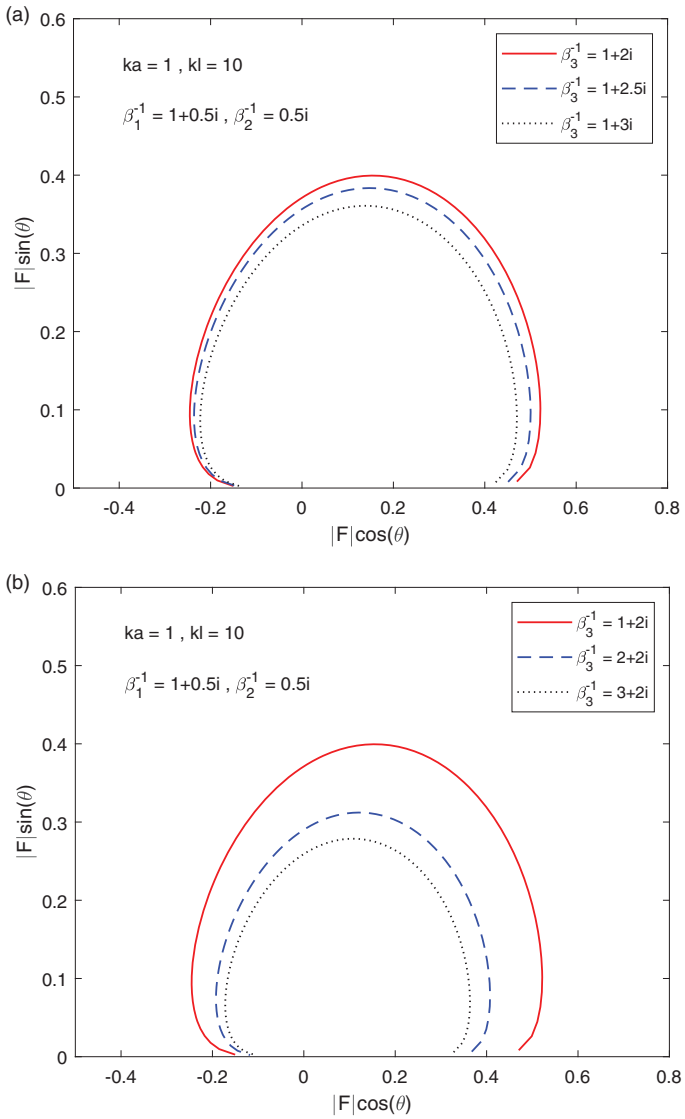

Figure 7. Amplitude of the diffracted field for different values of resistance $(\mathrm{Re}\beta_3^{-1})$ and reactance $(\mathrm{Im}\beta_3^{-1})$, respectively.

Computational results

In order to show the influence of the values of the surface admittances and the cavity on the diffracted field phenomenon, numerical results showing the variation of the amplitude of the diffracted field ($20\log|\mathcal{F}|$) with the observation angle are presented. The impedances $\beta^{-1}_{1,2,3}$, which are generally a complex number, determines the ability of a surface to guide and support the surface waves. $\beta^{-1}_{1,2,3} = \beta^{1}_{1,2,3} + i\beta^{2}_{1,2,3}$ where $\beta^{1}_{1,2,3}$ and $\beta^{2}_{1,2,3}$ correspond the resistance and reactance, respectively. Physically, the surface is lossless when the real part of

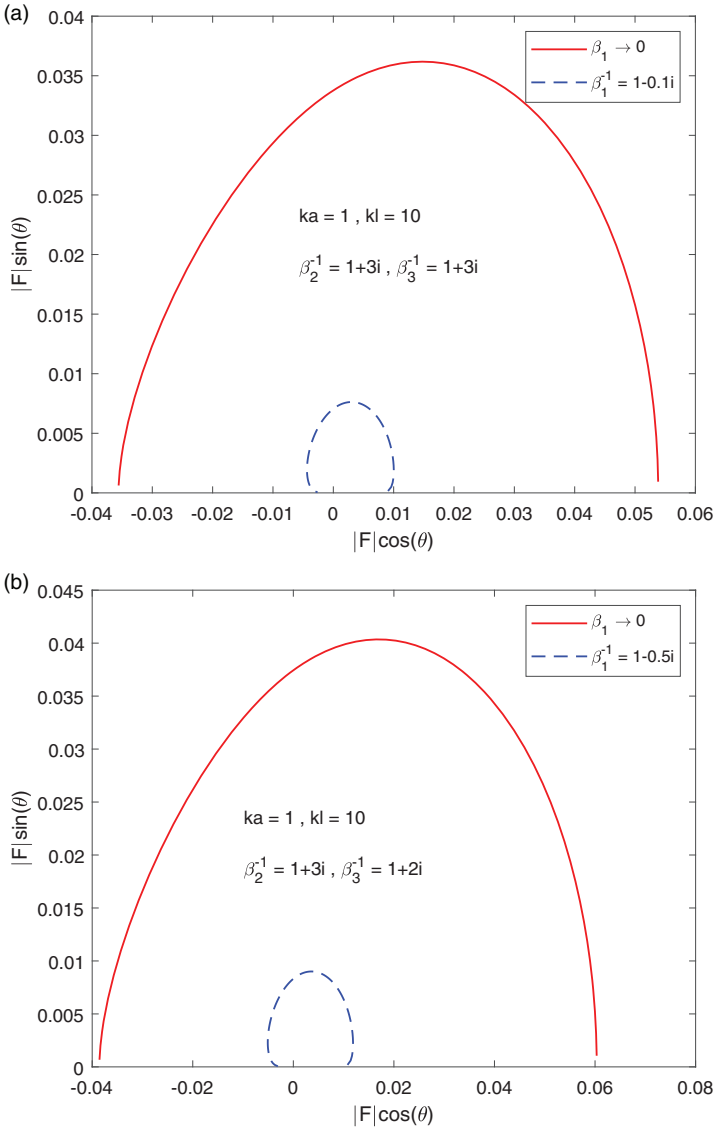

Figure 8. Amplitude of the diffracted field for different values of resistance ($\mathrm{Re}\beta_3^{-1}$) and reactance ($\mathrm{Im}\beta_3^{-1}$), respectively.

lining is zero and the surface waves can propagate on it without attenuation. The surface is lossy and surface wave is attenuated when real part is greater than zero. The imaginary part of lining can be positive or negative, then the surface is said to be capacitive or inductive, respectively.[20] Parameter values related with the surface linings are taken from the study of Demir et al.[12]; Tiryakioglu and Demir[18]; and Tiryakioglu.[20]

Figure 3 shows the variation of the diffracted field amplitude with the truncation number N. One can see that the amplitude of the diffracted field becomes insensitive to the truncation

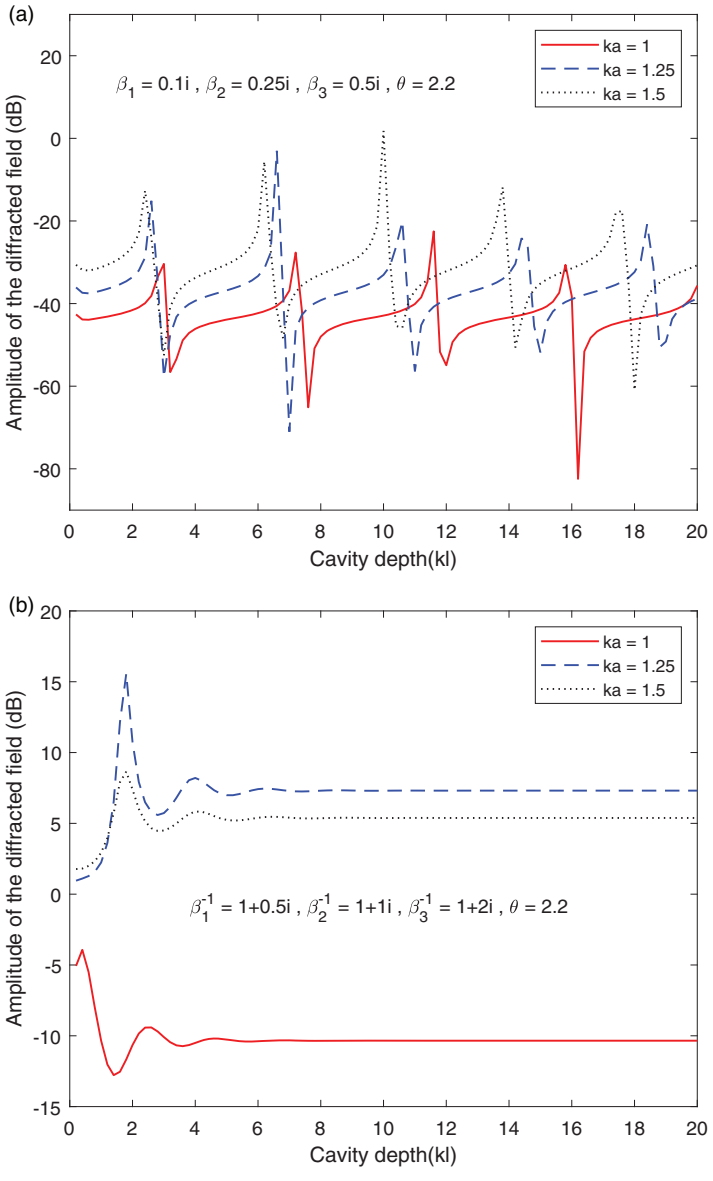

Figure 9. Diffracted field amplitude versus the cavity depth *kl* for different values of *ka*.

number N for $N \geqslant 20$, $ka = 1$, $kl = 10$, $\beta_1^{-1} = 1 + 0.5i$, $\beta_2^{-1} = 1 + 1i$, $\beta_3^{-1} = 1 + 2i$. In all numerical examples, N is chosen as $N = 20$.

In Figure 4, the amplitude of the diffracted field increases with the increasing value of ka for different values of admittances, as expected.

Figures 5 to 7 show the variation of the amplitude of the diffracted field for the values of resistance and reactance. As it can be seen that the diffracted field can be reduced by changing the values of $\mathrm{Im}\beta_1^{-1}$, $\mathrm{Im}\beta_2^{-1}$, $\mathrm{Im}\beta_3^{-1}$ and $\mathrm{Re}\beta_1^{-1}$, $\mathrm{Re}\beta_2^{-1}$, $\mathrm{Re}\beta_3^{-1}$.

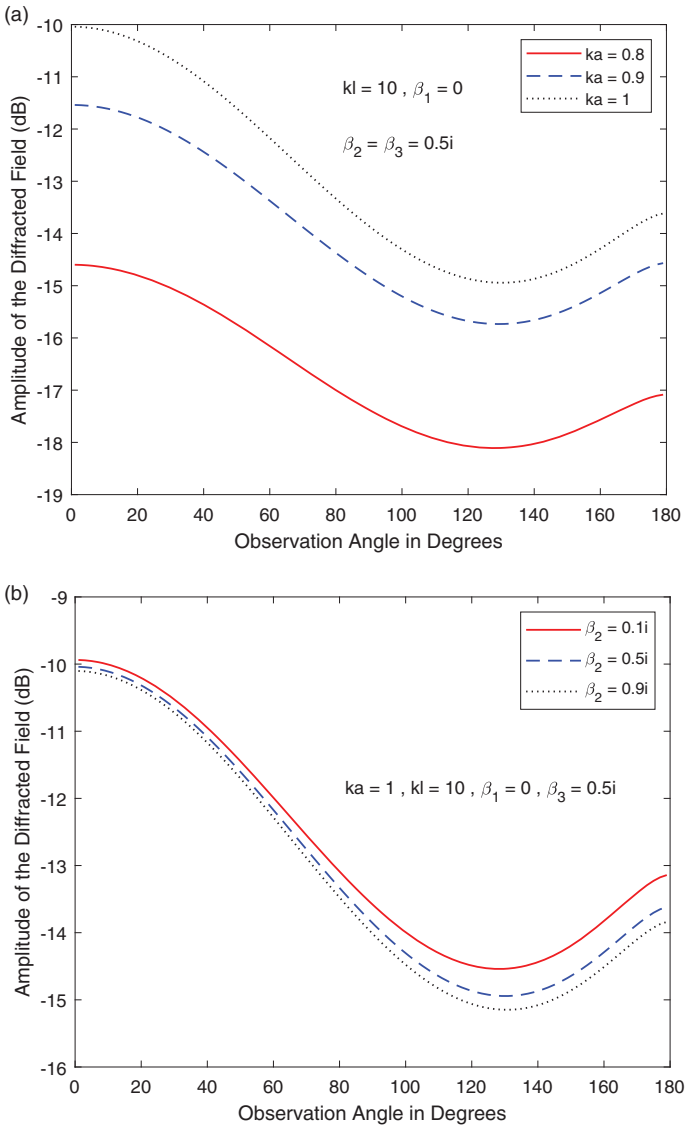

Figure 10. Comparison of the amplitude of the diffracted field with the study of Demir et al. (2002). Source: reproduced with permission from Demir et al. (2002).[12]

From Figures 5 to 7, one can see that the highest sound absorption can be achieved by choosing linings properly.

Figure 8 shows the variation of the amplitude of the diffracted field for the values of hard and soft outer surface of the cavity. It is seen that the diffracted field decreases significantly with outer lining compared to the rigid outer surface. Also, one can see that from Figure 8, an effect of outer lining, which is the main difference with previous study, is observed.

Figure 9 depicts the influence of the cavity depth kl on the diffraction phenomenon for different values of the cavity radius. It is observed that the diffracted field obtained in the second graph of Figure 9 is almost constant (no resonance effect) after $k = 5$, while the first graph of Figure 9 exhibits an oscillatory behavior. When the real part is zero, an oscillating behavior is observed. On the other hand, the resonance effect is lost when the real part is greater than zero.

Figure 10 shows an excellent agreement between the present paper ($\beta_1 = 0$) and the previous study.[12] In Figure 10, fundamental mode is used to compare with the previous study. Here, the impact of the incident field reduces to e^{-ikz} due to the fundamental mode ($m = 0$). Notice that the curve corresponding to $\beta_1 = 0$ coincides exactly with the result obtained in the previous paper by the authors[12] (Figures 4 and 5a). This comparison is also important for the accuracy of the mathematical results.

Concluding remarks

Diffraction of sound waves from a circular cylindrical cavity is presented rigorously. The Wiener–Hopf technique is engaged to obtain total diffracted field. Here, the outer surface is assumed to be lined with acoustically absorbing material which makes the problem more complicated. The problem is reduced Wiener–Hopf equation and solved by using the classical factorization and decomposition procedures. The solution involves two systems of linear algebraic equations involving two sets of infinitely many unknown expansion coefficients. Numerical results are obtained graphically for various values of the problem parameters.

As is well known, diffraction of the sound wave is reduced by the inner absorbing lining. In addition, the effect of the outer lining on the diffracted field is clearly seen from Figure 8.

The results are also compared with Demir et al.[12] and it is observed that the agreement is perfect. As a future work, a similar problem with the flow will be studied following the same method used here.

Declaration of conflicting interests

The author(s) declared no potential conflicts of interest with respect to the research, authorship, and/or publication of this article.

Funding

The author(s) received no financial support for the research, authorship, and/or publication of this article.

ORCID iD

Burhan Tiryakioglu https://orcid.org/0000-0003-1448-6147

References

1. Kobayashi K and Sawai A. Plane wave diffraction by an open-ended parallel plate waveguide cavity. *J Electromagnet Waves Appl* 1992; 6: 475–512.
2. Victoria A, Kimberly SR, Jonathan J, et al. Terahertz multichannel microfluidic sensor based on parallel-plate waveguide resonant cavities. *Appl Phys Lett* 2012; 100: 231108.
3. Tong Y and Pan J. Modal analysis of the scattering coefficients of an open cavity in a waveguide. *Wave Motion* 2017; 68: 242–252.
4. Porter R and Evans DV. Analysis of the effect of a rectangular cavity resonator on acoustic wave transmission in a waveguide. *J Sound Vib* 2017; 708: 138–153.
5. Rawlins AD. Radiation of sound from an unflanged rigid cylindrical duct with an acoustically absorbing internal surface. *Z Proc R Soc London, Ser A* 1978; 361: 65–91.
6. Hassan M and Rawlins AD. Sound radiation in a planar trifurcated lined duct. *Wave Motion* 1999; 29: 157–174.
7. Demir A and Buyukaksoy A. Radiation of plane sound waves by a rigid circular cylindrical pipe with a partial internal impedance loading. *Acta Acust United Ac* 2003; 89: 578–585.
8. Rienstra SW. Acoustic scattering at a hard-soft lining transition in a flow duct. *J Eng Math* 2007; 59: 451–475.
9. Tiryakioglu B and Demir A. Diffraction of acoustic waves by a semi-infinite pipe with finite impedance discontinuity. In: *4th international symposium on innovative technologies in engineering and science*, Antalya, Turkey, 2016, pp. 150–159.
10. Snakowska A, Jurkiewicz J and Gorazd L. A hybrid method for determination of the acoustic impedance of an unflanged cylindrical duct for multimode wave. *J Sound Vib* 2017; 396: 325–339.
11. Tiryakioglu B and Demir A. Radiation of sound waves from a semi-infinite rigid duct by local outer lining. In: *5th international symposium on innovative technologies in engineering and science*, Baku, Azerbaijan, 2017, pp. 1502–1511.
12. Demir A, Buyukaksoy A and Polat B. Diffraction of plane sound wave by a rigid circular cylindrical cavity with an acoustically absorbing internal surface. *Z Angew Math Mech* 2002; 82: 619–629.
13. Matsui E. Free-field correction for laboratory standard microphones mounted on a semiinfinite rod. *J Acoust Soc Am* 1970; 49: 1475–1483.
14. Kuryliak DB, Koshikawa S, Kobayashi K, et al. Wiener-Hopf analysis of the vector diffraction problems for a circular waveguide cavity. *Tech Rep IECE Japan* 2000: 73–80.
15. Kuryliak DB, Koshikawa S, Kobayashi K, et al. Wiener–Hopf analysis of the axial symmetric wave diffraction problem for a circular waveguide cavity. In: *Int workshop on direct and inverse wave scattering*, Gebze, Turkey, 2000, pp. 25–29.
16. Noble B. *Methods based on the Wiener-Hopf technique*. 2nd ed. New York, NY: Chelsea Publishing Company, 1988.
17. Watson GN. *A treatise on the theory of Bessel functions*. 2nd ed. London, UK: Cambridge University Press, 1944.
18. Tiryakioglu B and Demir A. Radiation analysis of sound waves from semi-infinite coated pipe. *Int J Aeroacoust* 2019; 18: 92–111.
19. Mittra R and Lee SW. *Analytical techniques in the theory of guided waves*. New York, NY: McMillan, 1971.
20. Tiryakioglu B. Sound radiation from the perforated end of a lined duct. *Acta Acust United Ac* 2019; 105: 591–599.